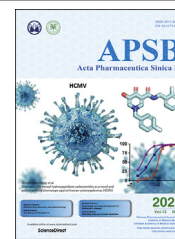




Chinese Pharmaceutical Association
Institute of Materia Medica, Chinese Academy of Medical Sciences

Acta Pharmaceutica Sinica B

www.elsevier.com/locate/apsb
www.sciencedirect.com



ORIGINAL ARTICLE

Prmt1 upregulated by *Hdc* deficiency aggravates acute myocardial infarction *via* NETosis



Zhiwei Zhang^{a,b,†}, Suling Ding^{a,†}, Zhe Wang^{c,†}, Xiaowei Zhu^a,
Zheliang Zhou^a, Weiwei Zhang^a, Xiangdong Yang^{a,c,d,e,*},
Junbo Ge^{a,c,d,e,*}

^aInstitutes of Biomedical Sciences and Shanghai Institute of Cardiovascular Diseases, Zhongshan Hospital, Fudan University, Shanghai 200032, China

^bReproductive Medicine Centre, Zhongshan Hospital, Fudan University, Shanghai 200032, China

^cDepartment of Cardiology, Zhongshan Hospital, Fudan University, Shanghai 200032, China

^dNHC Key Laboratory of Viral Heart Diseases, Fudan University, Shanghai 200032, China

^eKey Laboratory of Viral Heart Diseases, Chinese Academy of Medical Sciences, Shanghai 200032, China

Received 8 August 2021; received in revised form 20 September 2021; accepted 11 October 2021

KEY WORDS

PRMT1;
HDC;
Myocardial infarction;
Neutrophil extracellular
trap;
Transcriptomics;
Asymmetric
demethylation arginine

Abstract Neutrophils are mobilized and recruited to the injured heart after myocardial infarction, and neutrophil count has been clinically implicated to be associated with coronary disease severity. Histidine decarboxylase (HDC) has been implicated in regulating reactive oxidative species (ROS) and the differentiation of myeloid cells. However, the effect of HDC on neutrophils after myocardial infarction remains unclear. Here, we found that neutrophils were disorderly recruited into the ischemic injured area of the myocardium of *Hdc* deficiency (*Hdc*^{-/-}) mice. Moreover, *Hdc* deficiency led to attenuated adhesion but enhanced migration and augmented ROS/neutrophil extracellular traps (NETs) production in neutrophils. *Hdc*^{-/-} mouse-derived NETs promoted cardiomyocyte death and cardiac fibroblast proliferation/migration. Furthermore, protein arginine methyltransferase 1 (PRMT1) was increased in *Hdc*^{-/-} mouse-derived neutrophils but decreased with exogenous histamine treatment. Its expression could be rescued by blocking histamine receptor 1 (H1R), inhibiting ATP synthesis or reducing SWI/SNF chromatin remodeling complex. Accordingly, histamine or MS023 treatment could decrease ROS and NETs *ex vivo*, and ameliorated cardiac function and fibrosis, along with the reduced NETs in plasma *in vivo*. Together, our findings unveil the role of HDC in NETosis by histamine–H1R–ATP–SWI/SNF–PRMT1–ROS signaling and provide new biomarkers and targets for identifying and tuning the detrimental immune state in cardiovascular disease.

*Corresponding authors.

E-mail addresses: yang.xiangdong@zs-hospital.sh.cn (Xiangdong Yang), jbge@zs-hospital.sh.cn (Junbo Ge).

†These authors made equal contributions to this work.

Peer review under responsibility of Chinese Pharmaceutical Association and Institute of Materia Medica, Chinese Academy of Medical Sciences

<https://doi.org/10.1016/j.apsb.2021.10.016>

2211-3835 © 2022 Chinese Pharmaceutical Association and Institute of Materia Medica, Chinese Academy of Medical Sciences. Production and hosting by Elsevier B.V. This is an open access article under the CC BY-NC-ND license (<http://creativecommons.org/licenses/by-nc-nd/4.0/>).

1. Introduction

Myocardial infarction (MI) is one of the leading causes of death worldwide. After infarction, three sequential processes, inflammatory response, cardiomyocyte necrosis, and scar formation, determine the final ejection fraction and the survival rate of patients with MI^{1,2}. The inflammatory response, regulated by recruited immunocytes, including neutrophils, monocytes/macrophages, and lymphocytes, profoundly influences heart remodeling³.

Neutrophils, as sentinels of inflammation, first infiltrate the infarcted zone in great numbers after MI⁴. Although neutrophils have a relatively short lifespan, they secrete inflammatory mediators, purge debris of apoptotic cardiomyocytes⁵, and activate fibroblasts⁶.

A decade ago, neutrophils were found to form a net-like structure, containing double-stranded DNA, citrullination of histones and neutrophil granule protein, called neutrophil extracellular traps (NETs)⁷. Originally, NETs were regarded as the protection of our bodies from fungal and bacterial diseases. Recently, excessive NETs have been reported to be involved in the progression of other diseases, including atherosclerosis⁸, lupus erythematosus⁹, and coronavirus disease 2019 (COVID-19)¹⁰. NETs were also found in patients with MI/acute coronary syndromes, and the level of NETs in plasma was related to infarct size^{11,12}.

Histidine decarboxylase (HDC) catalyzes L-histidine to histamine and is involved in allergic responses, gastric acid secretion, immune modulation, and the development of hematopoietic stem cells¹³. In the bone marrow of mice, over 50% of CD11b⁺Ly6G⁺ granulocytic cells highly express HDC, and HDC-expressing granulocytes derived histamine plays important roles in the differentiation of immune cells¹⁴. Moreover, it has been reported that serum histamine concentrations significantly increased after MI, indicating the potential roles of HDC/histamine in MI¹⁵. However, the role of HDC/histamine in the regulation of neutrophils after MI has not been fully clarified.

In this study, we report that HDC plays a key role in regulating the functions of neutrophils. Recruitment, oxidative burst, and NETosis were significantly altered in *Hdc*^{-/-} mouse-derived neutrophils, which augmented the death of cardiomyocytes and the activation of fibroblasts. Blocking neutrophils to a certain extent could aid reduction of myocardial injury in *Hdc*^{-/-} mice. Furthermore, by using transcriptomics and proteomics, we found that aggravated cardiac injury in *Hdc*^{-/-} mice was due to excessive NETs through HDC—protein arginine methyltransferase 1 (PRMT1)—reactive oxygen species (ROS) pathway. The administration of exogenous histamine or the inhibitor of PRMT1 could ameliorate cardiac injury in *Hdc*^{-/-} mice.

2. Methods and materials

2.1. Animals and MI model

Hdc knockout (*Hdc*^{-/-}, BALB/c background) mice were generously provided by Professor Timothy C. Wang from Columbia University (New York, USA). The generation of *Hdc*^{-/-} mice has been described in previous papers¹⁶. The adopted *Hdc*^{-/-} mice in

the present work is the offspring of *Hdc*^{-/-} homozygous parents, generating not enough littermates as controls. Thus male wild-type (WT, in BALB/c background) mice at 8 to 12-week-old purchased from CAVENS. LA (Changzhou, China) were used as controls, which were shown the same phenotypes as WT littermates of *Hdc*^{-/-} mice, as previously described¹⁷. All procedures in this study were approved by the Institutional Review and Ethics Board of Zhongshan Hospital of Fudan University (Shanghai, China). The myocardial infarction model was performed as described before¹⁸. Briefly, male mice were anaesthetized with 3% isoflurane inhalation in a chamber. After exposing the hearts by left thoracotomy, a small incision was made at the fourth intercostal space to pop out the heart. The left main descending coronary artery (LCA) was permanently ligated at a site 3 mm from its origin. After the heart was placed back into the intrathoracic space, fast air evacuation and chest wall closure were performed. Histamine (Sigma, St. Louis, MO, USA) was injected with the dose of 4 mg/kg/day intraperitoneally (i.p.) beginning from 3 days before surgery and continuing until euthanasia. MS023 (MedChemExpress, Shanghai, China), the inhibitor of PRMT1 which has been used in *in vivo* tests⁶⁸, was injected 80 mg/kg i.p. every 3 days beginning from 3 days before surgery. For control groups, the same volume of phosphate buffered saline (PBS) was used. Anti-Ly6G antibodies and IgG isotype antibodies (BioXCell, Lebanon, NH, USA) were injected at 50 µg on Days 1, 3, and 5 post surgery.

2.2. Histopathological analysis

Hearts were embedded in optimal cutting temperature compound (O.C.T.; Sakura® Finetek Japan Co., Ltd., Tokyo, Japan) or in paraffin (Leica Biosystems, Wetzlar, Germany). 5 µm thick paraffin sections were used for stained with haematoxylin and eosin (H&E) and Masson's trichrome staining according to standard procedures.

Immunofluorescent staining was performed to detect neutrophil infiltration (neutrophil elastase and α -actinin, Abcam, Cambridge, UK) and NETs formation [anti-histone H3 citrulline R2+R8+R17, and myeloperoxidase (MPO), Abcam]. Co-staining was visualized by fluorescence microscope with 488- and 596-conjugated secondary antibodies (Abcam) mounted with fluoroshield mounting medium with 4',6-diamidino-2-phenylindole (DAPI, Abcam).

2.3. Enzyme-linked immunosorbent assay (ELISA) assay

CK-MB (Jiancheng Bioengineering Institute, Nanjing, China) and MPO (R&D Systems, Minneapolis, MN, USA) were measured with the respective ELISA kits, according to the manufacturer's instructions. Briefly, plasma samples were collected from mice in each group at the indicated time after MI, and centrifuged at 3000 ×g for 10 min, after which the supernatant was collected. The plasma of 100–200 µL was added into the 96-well plates for the measurement of concentrations based on the absorption values.

2.4. Neutrophil isolation

Mice neutrophils were harvested and purified as previously described¹⁹. In brief, bone marrow cells were gathered, added into Percoll gradient consisting of 52%, 65%, 78% Percoll layers (GE, Boston, MA, USA), and centrifuged at 2500 × g for 30 min at room temperature. The cells between 65% and 78% layers were harvested, and red blood cells were lysed with red blood cells lysis buffer (BD, New York, NY, USA).

2.5. Adult mouse cardiomyocyte and fibroblasts isolation

The isolation of adult mouse cardiomyocytes was performed as described previously²⁰. In brief, hearts of mice were incised, after injected with EDTA buffer from apical region of left ventricle. Then left ventricle was digested and disassociated to isolate cardiomyocytes and cardiac fibroblasts through gravity sedimentation. For hypoxia, the cardiomyocytes were placed in an anaerobic incubator filled with gas consisting of 1% O₂, 5% CO₂, and 94% N₂, at 37 °C for 24 h.

2.6. Adhesion assay

Isolated neutrophils were labeled with Calcein-AM (Thermo Fisher Scientific, Waltham, MA, USA) and plated on human umbilical vein endothelial cells (HUVEC) with the presence of 10 ng/mL tumor necrosis factor- α (TNF- α) as previously described²¹. Then wells were washed with PBS. The number of adhering neutrophils was counted, and the percentage was calculated.

2.7. Transwell migration assay

Neutrophil Transwell migration assay was performed as described previously²². Briefly, bone marrow derived neutrophils from each genotype were labeled with Calcein-AM, and seeded in serum-free RPMI 1640 medium in the upper chamber of Transwell inserts (BD Falcon, New York, NY, USA). Then recombinant interleukin-8 (IL-8, 100 ng/mL, Protein tech, Rosemont, IL, USA) were added in the lower chambers and incubated for 2 h at 37 °C in 5% CO₂ incubator. The migrated cells were analyzed by fluorescent microscopy.

2.8. Quantification of ex vivo NETs formation and ROS

The 5 × 10⁵ cells per well were seeded onto coverslips coated with poly-L-lysine (Beyotime, Nantong, China), and treated with phorbol myristate acetate (PMA, 200 nmol/L, MedChemExpress) for 18 h. Neutrophils were stained with DAPI/Sytox green (Thermo Fisher Scientific). Percentage values of NETs were calculated as the area of Sytox green positive cells relative to DAPI positive cells. The parameter was set to filter the Sytox green positive cells with small area to ignore the dead points of neutrophil for more accuracy.

To measure the level of ROS, isolated neutrophils were treated with DCFH-DA (MCE) for 30 min. Then cells were reconstituted with serum-free RPMI 1640 medium and transferred to black at 96-fold intervals, with or without PMA (200 nmol/L) treatment. The plate was measured at an excitation wavelength of 488 nm and an emission length of 530 nm using an automated plate monochrome reader (Molecular Devices, Silicon Valley, CA, USA).

2.9. TdT-mediated dUTP nick-end labeling (TUNEL) assay

TUNEL assay using the One Step TUNEL Apoptosis Assay Kit (Beyotime) was performed in cardiac tissue sections or cultured cardiomyocytes following the manufacturer's instructions. Briefly, cardiomyocytes were permeabilized with 0.05% Triton X-100 before labeling the segmented DNA of the apoptotic cells using TUNEL detection buffers. Then the samples were co-stained with anti- α -actinin primary antibody (CST, Danvers, MA, USA) followed by the Alexa Fluor-conjugated secondary antibodies (CST). Each staining in different groups was visualized with identical light exposure parameters under a fluorescence microscope (Leica Biosystems).

2.10. 5-Ethynyl-2-deoxyuridine (EdU) incorporation assay

EdU incorporation assay was analyzed by using BeyoClick™ EdU Cell Proliferation Kit (Beyotime) according to the manufacturer's instructions. In brief, isolated fibroblasts were incubated in DMEM (Thermo Fisher Scientific) with 10 μ mol/L EdU for 2 h at 37 °C/5% CO₂. After the incubation, the cells were washed with PBS to remove the DMEM and the free EdU probe. Then fibroblasts were fixed in 4% paraformaldehyde at room temperature and stained with vimentin primary antibody (CST) followed by the Alexa Fluor-conjugated secondary antibodies (CST).

2.11. Cell migration assay/wound healing

Fibroblasts labeled with Calcein-AM were seeded in 24-well plates and cultured until cell monolayers formed. Monolayers were wounded by manual scraping with a 10 μ L micropipette tip. The cells were then incubated with NETs from neutrophils of each genotype pretreated with PMA for 4 h. Wound repair was analyzed through measuring the injured area recovered from the wounding borders.

2.12. DNA accessibility (DNase I sensitivity) assay

DNA accessibility assay were carried out as described previously²³. In brief, DNA from HL60 cells treated with histamine for 12 h was digested by DNase I (Takara, Kyoto, Japan) and accessed by quantitative real-time PCR (qRT-PCR).

2.13. ELISA for MPO–DNA complexes

Capture ELISA was used to measure the MPO/NA complexes as described²⁴. Briefly, capture antibody for myeloperoxidase (R&D Systems) was diluted and added into an ELISA plate overnight. After blocking, diluted plasma samples were added to the plate overnight. The supernatant was discarded, and diluted PicoGreen (Thermo Fisher Scientific) with 1× Tris-EDTA (TE) buffer was added to the plate. Fluorescence of the samples was measured using an automated plate monochrome reader (Molecular Devices).

2.14. Measurement of DNA concentrations

DNA concentrations were measured using the Quant-iT PicoGreen dsDNA assay kit (Thermo Fisher Scientific) following the manufacturer's instructions. In brief, plasma was mixed with the PicoGreen dye, added to the microplate wells, and then incubated

in the dark for 10 min. The fluorescence of the samples was measured using an automated plate monochrome reader (Molecular Devices)²⁴.

2.15. Statistical analysis

Data are shown as mean \pm standard error of mean (SEM) of at least three independent experiments for each cellular experimental group and at least five independent experiments for each animal group. The size and count of NETs or cells were accessed by Python using OpenCV (<https://github.com/Winston-00/NET-analysis>). We evaluated the data with Student's *t*-test for two-group comparisons, and one or two way analysis of variance for multiple comparisons. The value of $P < 0.05$ was considered statistically significant.

3. Results

3.1. Transcriptomic profiling of *Hdc*^{-/-} mice with deteriorative outcomes after MI

To elucidate the role of histamine deficiency in myocardial infarction, we compared the severity of myocardial infarction injury between *Hdc*^{-/-} and WT (*Hdc*^{+/+}) mice. As expected, the levels of CK-MB increased significantly on Day 1 after MI in both *Hdc*^{-/-} and *Hdc*^{+/+} mice (Fig. 1A). However, the level of CK-MB in the plasma of *Hdc*^{-/-} mice was much higher than that in *Hdc*^{+/+} mice (Fig. 1A), indicating that *Hdc* deficiency aggravated cardiomyocyte death. Furthermore, cardiac function on Day 7 after MI surgery was measured by echocardiography. The results demonstrated that the ejection fraction (EF) and fractional shortening (FS) (Fig. 1B and C, and Supporting Information Fig. S1A for the representative images) in *Hdc*^{-/-} mice were significantly lower than those in *Hdc*^{+/+} mice. These data indicated that *Hdc* deficiency was associated with poor prognosis after MI.

To investigate the detailed mechanisms underlying the deteriorated cardiac functions in *Hdc*^{-/-} mice after MI, RNA-sequencing was performed to dissect the transcriptomic profile of hearts from *Hdc*^{+/+} and *Hdc*^{-/-} mice on Days 0, 1 and 7 after MI (Fig. 1D). A total of 259 genes and 273 genes were identified as differentially expressed genes (DEGs, $P < 0.05$, FC > 1.5) in the hearts of *Hdc*^{+/+} and *Hdc*^{-/-} mice on Days 1 and 7 after MI. Among them, 92 genes were consistently abnormally expressed both on Day 1 and on Day 7 after MI (Fig. 1E).

To identify the specific biological process (BP) and networks involved in the progression of MI, we performed gene ontology (GO) enrichment analysis with the Day 1 and Day 7 DEGs, respectively. The top 15 GO terms were enriched based on the DEGs and their changes are shown in the time course. In the GO analysis of BP, more than 50% of the top terms were related to the function of immune cells, including leukocyte chemotaxis, leukocyte migration, and regulation of the inflammatory response (Fig. 1F). The DEGs with leukocyte migration/chemotaxis and regulation of the inflammatory response were diminished at the 7th day of MI, while genes with T cell activation were augmented. In the GO analysis of cellular component (CC), DEGs were related to cell vesicles, including lysosomes, lytic vacuoles, and secretory granules (Fig. 1G). In the GO analysis of molecular function (MF), lists of genes were generated in the categories of amide binding, ATPase activity, coenzyme binding, and cytokine receptor binding (Fig. 1H). In general, the DEGs were mainly

involved in immune cell function, including chemotaxis/migration, secretory granule production, and other inflammatory responses. These results suggested that immune processes likely play a vital role in the pathological progression of MI and subsequent heart remodeling.

3.2. Infiltration of immune cells especially neutrophils was shifted in *Hdc*^{-/-} mice

The contribution of immunological phenomena to cardiac diseases is of particular clinical relevance²⁵. Great numbers of immunocytes successively infiltrate the infarcted zone after MI, influencing the subsequent process of myocardial healing. The results of H&E staining confirmed that there were many inflammatory cells infiltrating into the infarcted zone (Fig. 2A). Therefore, we estimated the pattern of the infiltrated immunocytes by employing the MCP counter algorithm. As shown in Fig. 2B, the infiltration of immunocytes, including neutrophils, monocytes, dendritic cells (DCs), B cells, and T cells, in the infarcted hearts, was changed after *Hdc* deletion. As *Hdc* is expressed in myeloid cells, especially in Ly6G⁺ granulocytes, we further focused on exploring the consequence of *Hdc* deficiency in neutrophils responding to ischemia injury. As flow cytometry data (Fig. 2C and Supporting Information Fig. S2A for the gating strategy) revealed, the number of infiltrated neutrophils in the infarcted zone peaked on Day 1 and greatly dropped on Days 3 and 7 after MI. However, there were still many more neutrophils in the cardiac infarcted zone of *Hdc*^{-/-} mice than in *Hdc*^{+/+} mice on Days 3 and 7 after MI. The immunostaining result was consistent with the flow cytometry data (Fig. 2D and E).

To figure out whether the increased neutrophils contributed to the aggravated cardiac injury of *Hdc*^{-/-} mice, the anti-Ly6G antibody was applied to neutralize neutrophils after myocardial infarction. The EF and FS in *Hdc*^{-/-} mice were improved by the administration of anti-Ly6G antibody but not IgG (Fig. 2F). Similarly, compared with IgG, anti-Ly6G antibody reduced the cardiac fibrosis of *Hdc*^{-/-} mice (Fig. 2G). These findings suggested that *Hdc* deficiency-aggravated myocardial injury after MI may be due to the effect of *Hdc* deficiency mainly on the regulation of neutrophils.

3.3. *Hdc* deficiency dysregulates the characteristic cellular activities of neutrophils

In a previous study, *Hdc* deficiency was proposed to promote phagocyte infiltration in infectious inflammation²⁶. Nevertheless, little is known about its role in sterile inflammation. We first investigated the effect of *Hdc* deficiency on the adhesion and migration of neutrophils. Compared with *Hdc*^{+/+} neutrophils, *Hdc*^{-/-} neutrophils showed significantly decreased adhesion to HUVECs after stimulation with TNF- α (Fig. 3A). However, *Hdc*^{-/-} neutrophils have a higher migration ability with the attraction of IL-8 through Transwells (Fig. 3B). These data indicated that *Hdc* deficiency led to disordered neutrophil priming in a sterile inflammatory environment.

The response of neutrophils to stimulation relies on the production of ROS and the formation of NETs under both infectious and sterile inflammatory conditions. Therefore, we investigated whether *Hdc* affected the generation of ROS in neutrophils by flow cytometry. Regardless of PMA treatment, *Hdc*^{-/-} neutrophils produced significantly higher levels of ROS than *Hdc*^{+/+} neutrophils did (Fig. 3C). Accumulating studies have reported

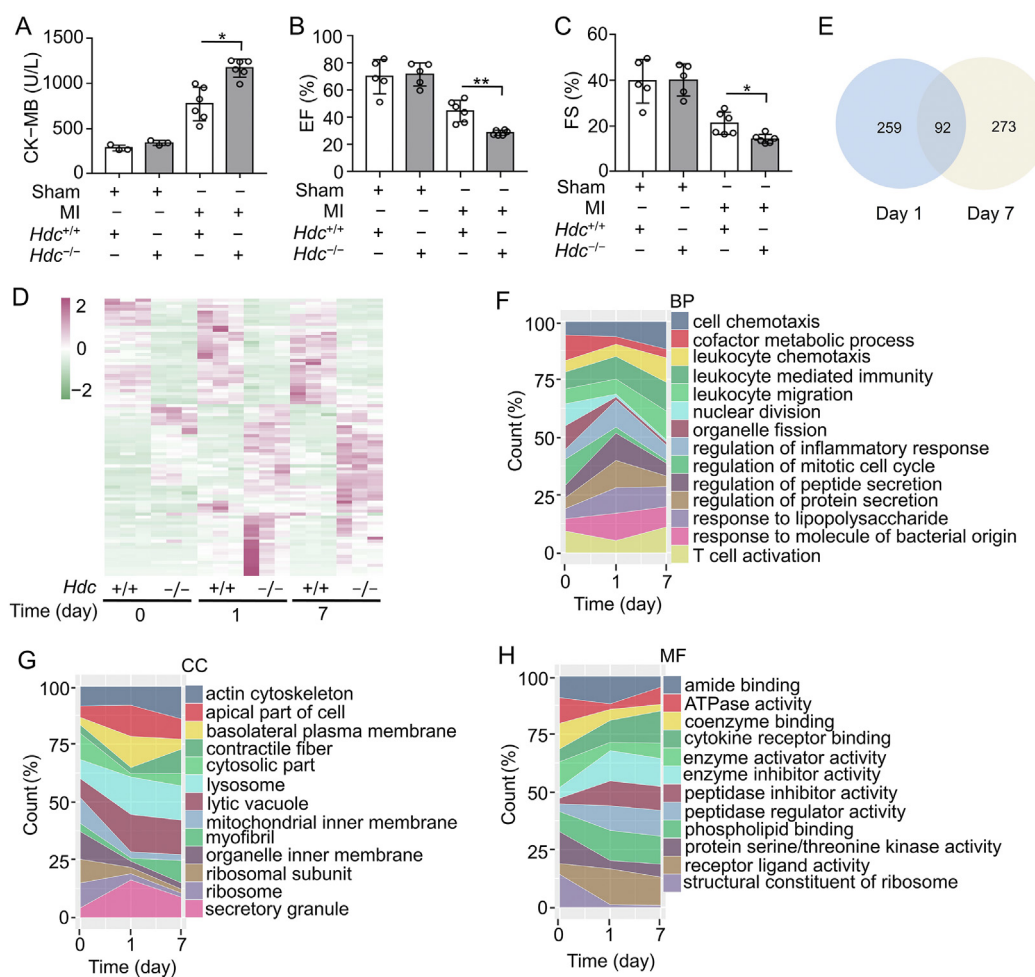


Figure 1 *Hdc* deficiency aggravates infarct injury and alters the cardiac transcriptome after MI. (A) Plasma levels of CK-MB from *Hdc*^{-/-} and *Hdc*^{+/+} mice on Day 1 after ligation were determined by ELISA according to the manual instructions. (B and C) Quantitation of left ventricle ejection fraction (EF) and fractional shortening (FS) of *Hdc*^{-/-} and *Hdc*^{+/+} mice on the 7th day after infarction. Data are shown as mean \pm SEM ($n = 6-8$ mice in each group). * $P < 0.05$, ** $P < 0.01$. (D and E) Gene expression profiling of hearts from *Hdc*^{+/+} and *Hdc*^{-/-} mice on Days 0, 1, and 7 after MI respectively. The heatmaps depicts up/down-regulated differentially expressed genes (DEGs) at the indicated time point (D). The number of DEGs and the overlap genes consistently differentially expressed on Days 1 and 7 after MI were shown in Venn diagram (E). $n = 3$ per group. (F-H) gene ontology (GO) analysis of DEGs between *Hdc*^{-/-} and *Hdc*^{+/+} mice. The top 15 GO terms of biological process (BP, F), cellular component (CC, G) and molecular function (MF, H) at the indicated time points were shown.

that excessive ROS promote the formation of NETs, which is a unique way of exacerbating peripheral cell death²⁶. Therefore, we assessed the areas of NETs formation under PMA treatment. Bone marrow-derived neutrophils from *Hdc*^{-/-} mice, after treatment with PMA *in vitro*, were shown to have a larger area of Sytox green-positive cells that represented NETs (Fig. 3D and E).

Furthermore, although there was no significant difference in the number of neutrophils infiltrating into the infarcted zone on Day 1 after MI in *Hdc*^{+/+} and *Hdc*^{-/-} mice as shown in Fig. 2, the co-staining of neutrophil elastase and citrullinated histone H3 revealed that there were much more NETs in the cardiac infarcted zone of *Hdc*^{-/-} mice even on Day 1 after MI, compare with *Hdc*^{+/+} mice (Fig. 3F and G). These results indicated that *Hdc* played an essential role in regulating the characteristic cellular activities of neutrophils, which may be involved in the more severe pathological progression of MI in *Hdc*^{-/-} mice.

3.4. *Hdc* deficiency in neutrophils promotes cardiomyocyte death and cardiac fibroblast proliferation/migration through NETosis

Hdc deficiency in neutrophils affected the cellular activities of neutrophils, as observed above. Next, we investigated the effects of neutrophils on cardiomyocytes. Neutrophils isolated from the bone marrow of *Hdc*^{+/+} or *Hdc*^{-/-} mice were co-cultured with cardiomyocytes for 24 h under hypoxia condition after activated by PMA. The TUNEL assay data demonstrated that *Hdc*^{-/-} neutrophils caused more cardiomyocyte death than *Hdc*^{+/+} neutrophils did (Fig. 4A). However, the difference was abolished by treatment with DNase I, which could disrupt the structure of NETs. Moreover, by staining with citH3 and TUNEL in cardiac sections, the *in vivo* study revealed that there were more NETs accompanied by more cardiomyocyte death on Day 1 after MI in *Hdc*^{-/-} mice (Fig. 4B) than in *Hdc*^{+/+} mice, indicating a positive relationship between NETs

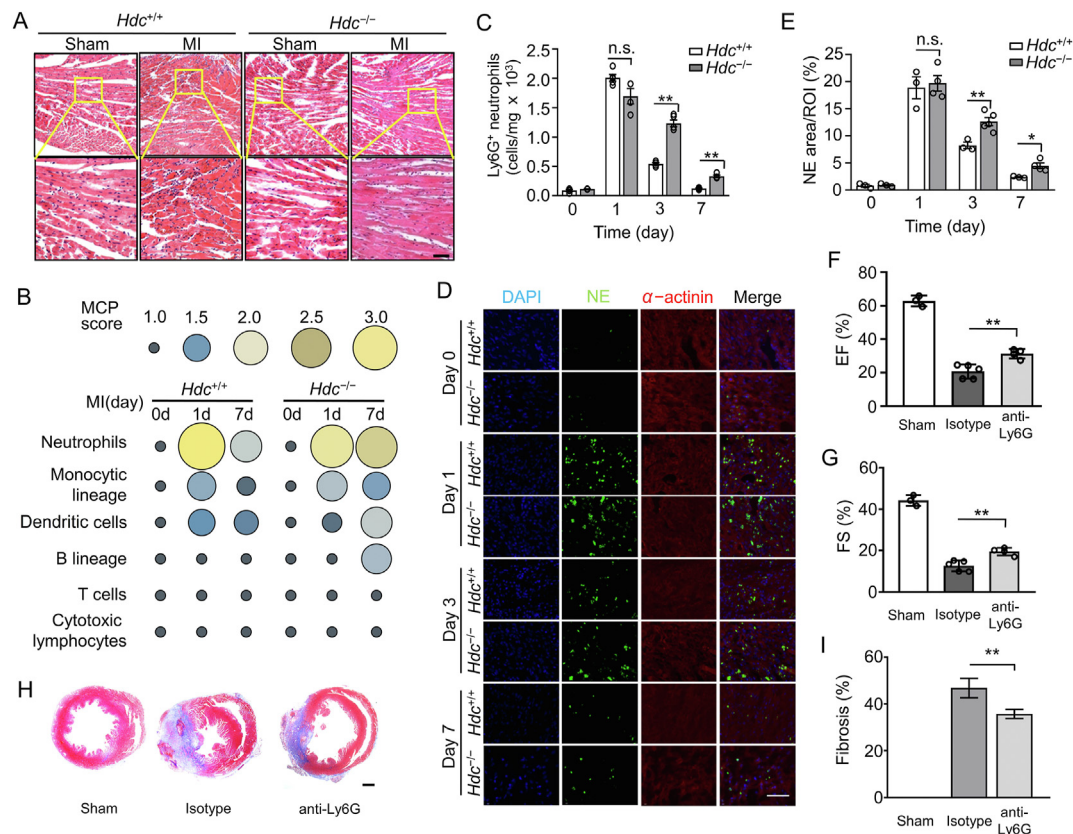


Figure 2 *Hdc* deficiency changed the pattern of the infiltrated immune cells in particular of neutrophil in infarcted zone after MI. (A) Representative pictures of H&E staining of hearts from *Hdc*^{+/+} and *Hdc*^{-/-} mice on Day 1 after MI surgery. (B) The size and the color indicate the MCP count score of the indicated immunocytes infiltrating into hearts on Days 1 and 7 after MI ($n = 4-5$). (C) Flow cytometry analysis of the numbers of Ly6G⁺ neutrophils in the hearts of *Hdc*^{-/-} and *Hdc*^{+/+} mice on Days 1 and 7 after MI or sham operation. (D) Representative images of immunofluorescence staining of neutrophil elastase (NE) and α -actinin in the infarct border zone on Days 1 and 7 after MI or sham operation. (E) Quantification of NE positive neutrophils in the infarct border zone. $n = 3-5$ per group. (F) Quantitation of left ventricle ejection fraction (LVEF) and FS of *Hdc*^{-/-} mice injected with anti-Ly6G antibody or its isotype after infarction. $n = 3-5$ mice in each group. (G) Representative images and quantitation of Masson staining of hearts from *Hdc*^{-/-} mice injected with anti-Ly6G antibody or its isotype on Day 7 after infarction. $n = 3-5$ mice in each group. Data are shown as mean \pm SEM. * $P < 0.05$, ** $P < 0.001$. n.s., no significant. Scale bar, 50 μ m.

and cardiomyocyte death. These findings suggest that *Hdc* deletion in neutrophils promoted cardiomyocyte death through NETosis.

Studies have reported that excessive NETs can induce fibrosis²⁷⁻²⁹, which participates in multiple pathological processes. Thus, we explored whether *Hdc* deficiency altered the effect of neutrophils on cardiac fibroblasts. Cardiac fibroblasts were co-cultured with *Hdc*^{+/+} or *Hdc*^{-/-} mouse-derived NETs. An EdU incorporation assay was employed to determine the proliferation of cardiac fibroblasts. The results revealed that *Hdc*^{-/-} neutrophils boosted the proliferation of fibroblasts to a higher degree than *Hdc*^{+/+} neutrophils did (Fig. 4C). However, when treated with DNase I simultaneously, the ability of NETs to promote the proliferation of fibroblasts was diminished to similar levels in both groups (Fig. 4C). Next, we performed wound healing assays to investigate the influence of *Hdc*^{+/+} and *Hdc*^{-/-} NETs on the migration of fibroblasts. The migration of fibroblasts co-cultured with *Hdc*^{-/-} NETs was faster than that of fibroblasts co-cultured with *Hdc*^{+/+} NETs (Fig. 4D). Similarly, DNase I treatment decreased the migration ability of both groups to the same degree (Fig. 4D). All these results demonstrated that *Hdc* deficiency in neutrophils exerted its pro-effect on cardiomyocyte death and fibroblast proliferation and migration by NETosis.

3.5. *PRMT1* is negatively regulated by histamine in myeloid cells

To unveil the mechanism through which *Hdc* regulates NETosis, we first sorted CD11b positive cells from the bone marrow of *Hdc*^{-/-} or *Hdc*^{+/+} mice for microarray analysis and then screened out the DEGs regulated by *Hdc* deficiency or histamine, through combining our data and published myeloid cell transcriptome data from other research groups.

Differential gene analysis revealed that there were 3096 DEGs between the *Hdc*^{+/+} and *Hdc*^{-/-} groups, and 1551 DEGs between groups with or without histamine treatment (Fig. 5A). Additionally, according to a previous study³⁰, there were 2628 DEGs between the *Hdc*-high expression group (*Hdc*-GFP^{high}) and the *Hdc*-low expression group (*Hdc*-GFP^{low}) (Fig. 5A). Among them, 64 DEGs were overlapped in the three groups (Fig. 5A). Their relative expression levels were shown in the heatmaps (Fig. 5B).

Among the 64 DEGs, we noted that the expression level of *Prmt1* was downregulated in the histamine group and *Hdc*-GFP^{high} group but augmented in the *Hdc*^{-/-} group (Fig. 5C). PRMT1 is a protein arginine methyltransferase that has been reported to methylate a variety of protein substrates, including

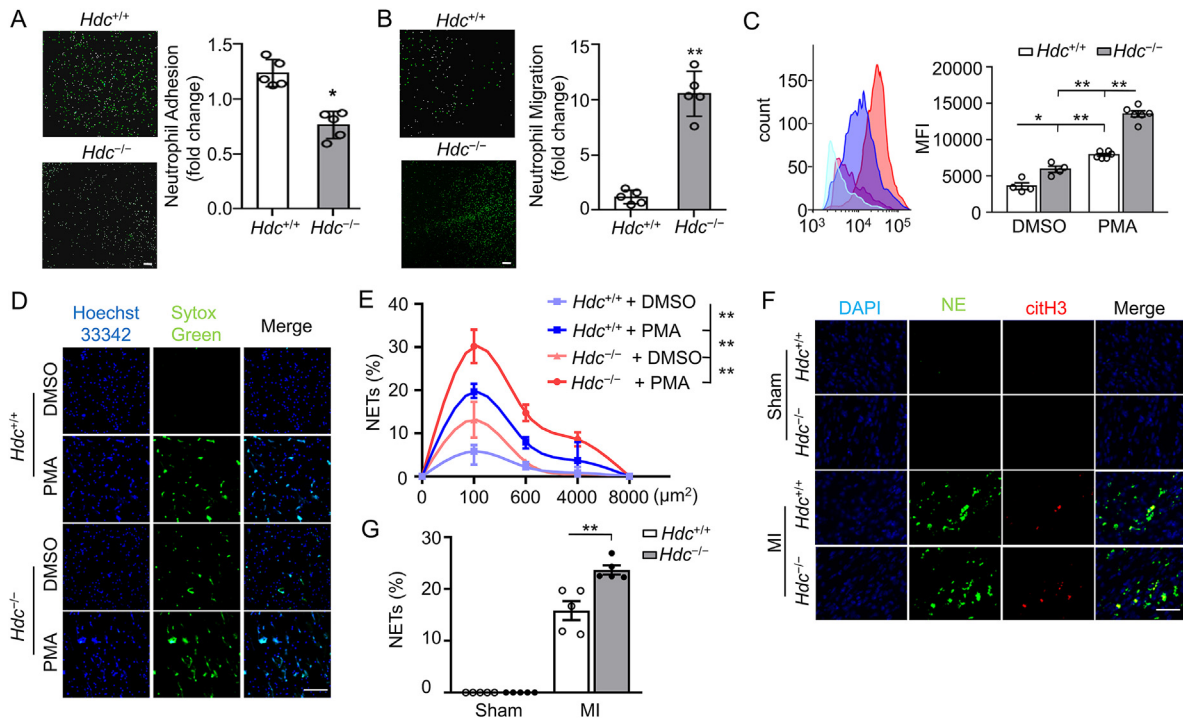


Figure 3 *Hdc* deficiency dysregulates the characteristic cellular activities of neutrophils. (A) Calcein-AM-labeled neutrophils isolated from the bone marrow of *Hdc*^{-/-} and *Hdc*^{+/+} mice were incubated with HUVECs. The percentage values of Calcein-AM⁺ adherent cells were measured after washing ($n = 4$). (B) Calcein-AM-labeled neutrophils isolated from the bone marrow of *Hdc*^{-/-} and *Hdc*^{+/+} mice were cultured in Transwell plate to assess migration capacity. Green fluorescence showed the migrated cells across Transwell ($n = 4$). (C) FACS analysis of the generation of ROS in *Hdc*^{-/-} and *Hdc*^{+/+} mice derived neutrophils before and after PMA treatment ($n = 4-6$). (D) Representative pictures of immunofluorescence staining of *Hdc*^{-/-} and *Hdc*^{+/+} neutrophils after exposure to PMA for 18 h with Sytox green and Hoechst 33342 (blue). (E) The areas of Sytox green⁺ NETs derived from *Hdc*^{-/-} and *Hdc*^{+/+} neutrophils were quantified ($n = 4$). (F) Representative images of immunofluorescence co-staining of NE (green), citH3 (red), and DAPI (blue) in cardiac slices of *Hdc*^{-/-} and *Hdc*^{+/+} mouse on Days 1 and 7 after MI or sham operation ($n = 4-5$). (G) Percentage values of neutrophils with evidence of NET formation (NE⁺/citH3⁺) in the cardiac slices of *Hdc*^{-/-} and *Hdc*^{+/+} mice were analyzed ($n = 5$). Data are shown as mean \pm SEM. * $P < 0.05$, ** $P < 0.01$. Scale bar: 50 μm .

those involved in gene transcription, DNA damage repair, signal transduction, and protein translocation³¹.

To verify the alteration of *Prmt1* level in myeloid cells, we firstly detected its expression in neutrophils. Data showed that the level of *Prmt1* was transcriptionally and translationally increased in *Hdc*^{-/-} mouse-derived neutrophils (Fig. 5D and Supporting Information Fig. S3A).

To test whether the expression of PRMT1 is regulated by histamine in granule cell like HL60 cells, the concentration gradient and time course assay were performed on HL60 cells. Our data show that the expression of PRMT1 was decreased responding to the treatment of 10 and 100 $\mu mol/L$ histamine (Fig. 5E). And it began to decrease at 6 h after histamine treatment, kept for more than 72 h (Fig. 5F and Fig. S3B).

Next, we investigated the expression of other members of PRMT family, with the treatment of histamine. As shown in Fig. S3C, only PRMT1, with the greatest Ct value, has been downregulated among PRMT1-6, after the treatment with histamine.

To verify whether the enhanced ROS generation and NETosis caused by *Hdc* deficiency in neutrophils were mediated through PRMT1, we inhibited the activity of PRMT1 using MS023. MS023 is the specific type I inhibitor of PRMTs, which had been reported to be applied in treating acute myeloid leukemia (AML)

in a relatively low dose³². To minimize its side effects, we had chosen the optimal concentration of MS023 on PRMT1 according to the reported C50 of MS023 on PRMT1. The data showed that the increased production of ROS and the augmented formation of citH3-positive NETs in *Hdc*^{-/-} neutrophils were reduced after 24 h of treatment with MS023 or histamine (Fig. 5G and H).

3.6. Histamine repressed the transcription of PRMT1 by restricting the DNA accessibility of the transcriptional start site (TSS) region of PRMT1

There are four known histamine receptors (H1R, H2R, H3R, and H4R) expressed in myeloid cells, and we wondered which of them would be responsible for the repression of histamine on PRMT1 in neutrophils. Among the inhibitors of four histamine receptors, only the H1R antagonist pirlamine rescued the decrease of PRMT1 induced by histamine treatment in HL60 cells (Fig. 6A), suggesting that the regulation of PRMT1 by histamine was dependent on H1R.

Next, we explored the mechanism by which histamine inhibited the expression of PRMT1. Since PRMT1 was decreased at the mRNA level, suggesting the regulation of its expression at the transcriptional level, we attempted to identify the key transcription factors of PRMT1. Signal transducer and activator of

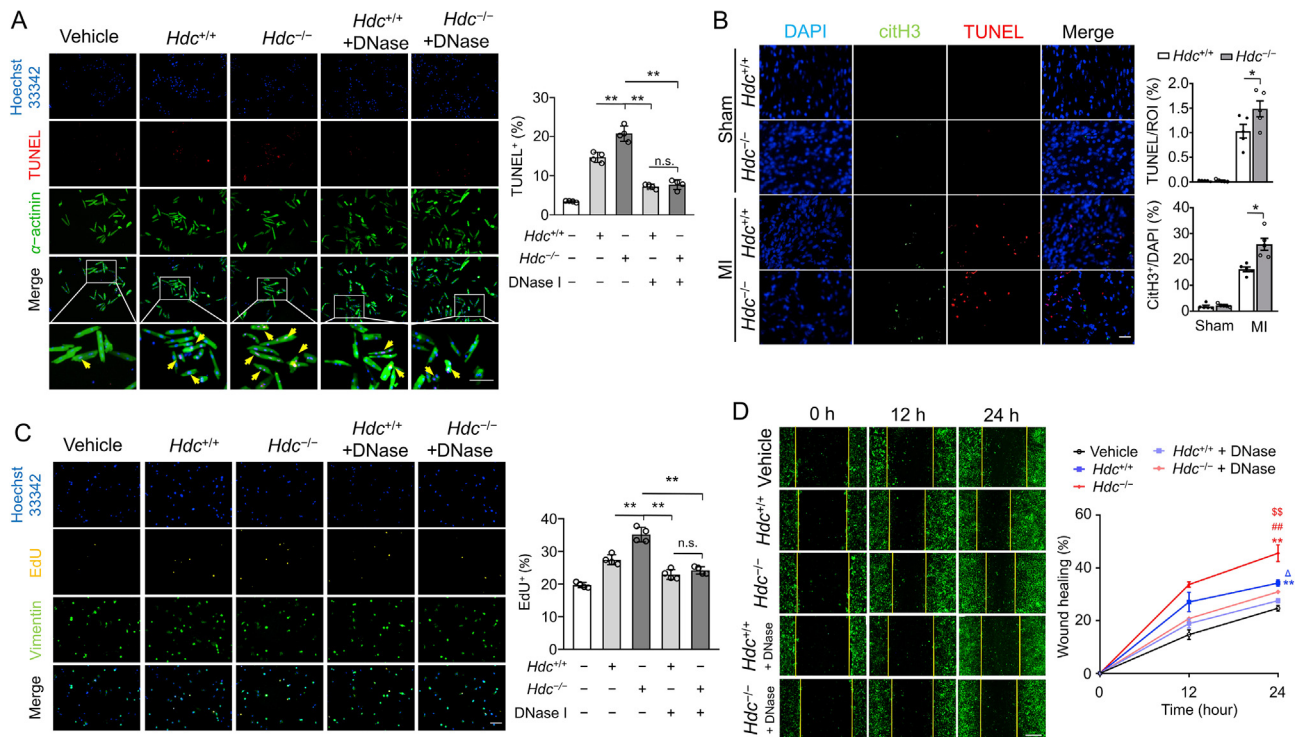


Figure 4 *Hdc* deficiency in neutrophils augments cardiomyocytes death and cardiac fibroblasts proliferation/migration through NETosis. (A) Representative images of TUNEL assay of cardiomyocytes treated with NETs from *Hdc*^{-/-} and *Hdc*^{+/+} neutrophils under hypoxia condition. DNase I was employed to interrupt the structure of NET. TUNEL positive cells are shown in red. α -Actinin positive cardiomyocytes are displayed as green. Nucleus is stained with Hoechst 33342, in blue. Percentage values of TUNEL⁺ cells were calculated and are shown as mean \pm SEM ($n = 4-5$). $^{**}P < 0.01$; n.s., no significant. (B) Representative images of immunofluorescence co-staining of citH3 (green), TUNEL (red) and DAPI (blue) in cardiac slices of *Hdc*^{-/-} and *Hdc*^{+/+} mice on Day 1 after MI or sham operation. The percentage values of citH3⁺ NETs and TUNEL⁺ cells were quantified and are shown as mean \pm SEM ($n = 5$). $^{*}P < 0.05$. (C) Representative images of EdU (red), Vimentin (green), DAPI (blue) co-staining for fibroblasts treated with NETs from *Hdc*^{-/-} and *Hdc*^{+/+} neutrophils. DNase I was employed to interrupt the formation of NETs. The percentage values of EdU⁺ cells were calculated and are shown as mean \pm SEM ($n = 4-5$). $^{**}P < 0.01$; n.s., no significant. (D) Representative images of fibroblast migration assay. A confluent monolayer of fibroblasts was scraped with 200 μ L pipette tip and co-cultured with NETs from *Hdc*^{-/-} and *Hdc*^{+/+} neutrophils for 24 h. DNase I was employed to interrupt the formation of NETs. The ratios of wound healing were quantified and are shown as mean \pm SEM ($n = 3$). $^{**}P < 0.01$ vs. vehicle group; $^{\Delta}P < 0.05$ vs. *Hdc*^{+/+} + DNase; $^{\#}P < 0.01$ vs. *Hdc*^{+/+} group; $^{\$}P < 0.01$ vs. *Hdc*^{-/-} group. Scale bar: 50 μ m.

transcription 1 (STAT1) and CCAAT enhancer binding protein beta (CEBPB) have been reported to bind to the promoter region of *PRMT1* in fibroblasts^{33,34}. However, knocking down *STAT1* or *CEBPB* in HL60 cells did not abolish the repressive effect of histamine on the level of *PRMT1* mRNA in HL60 cells (Fig. 6B), which indicated that there was a unique transcriptional mechanism different from those in known cell types during the process of histamine repressing the transcription of *PRMT1*.

To further characterize the pathway by which histamine regulates *PRMT1* expression, DNA accessibility was assessed by DNase digestion assay. The data revealed that TSS of *PRMT1* became DNase I resistant after histamine treatment (Fig. 6C and D).

Since the ATP-dependent SWI/SNF complex contributes to chromatin remodeling³⁵, we tested whether it was involved in the regulation of *PRMT1*. Silencing the catalytic subunits of the SWI/SNF complex, Brahma (BRM) and Brahma related gene 1 (BRG1), abolished the repressive effect of histamine on the expression of *PRMT1* (Fig. 6E). Similarly, with oligomycin treatment, which inhibited ATP production, the repression of histamine on the mRNA level of *PRMT1* was rescued (Fig. 6F). In

general, these findings revealed that HDC/histamine down-regulated the transcription of *PRMT1* by restricting the DNA accessibility of *PRMT1* in an ATP-SWI/SNF-dependent manner.

3.7. Asymmetric arginine dimethylation profiling of *PRMT1* targets are regulated by histamine

To further identify the downstream proteins methylated by *PRMT1*, the proteins with asymmetric dimethylated arginine (ADMA) were harvested by co-immunoprecipitation (co-IP) with ADMA antibody from the lysate of cells with or without histamine treatment. Co-massie blue staining showed that there was a significant decrease in the level of proteins with ADMA responding to histamine treatment (Fig. 7A and Supporting Information Fig. S4A).

Then, we performed mass spectrometry to identify the profile of the proteins with ADMA before and after histamine treatment. There were 1488 proteins detected in the group without histamine treatment and 1392 proteins detected in the group with histamine treatment. Among them, 339 unique proteins existed in the former, while 243 proteins uniquely existed in the latter (Fig. 7B and Table 1³⁶⁻⁴⁹).

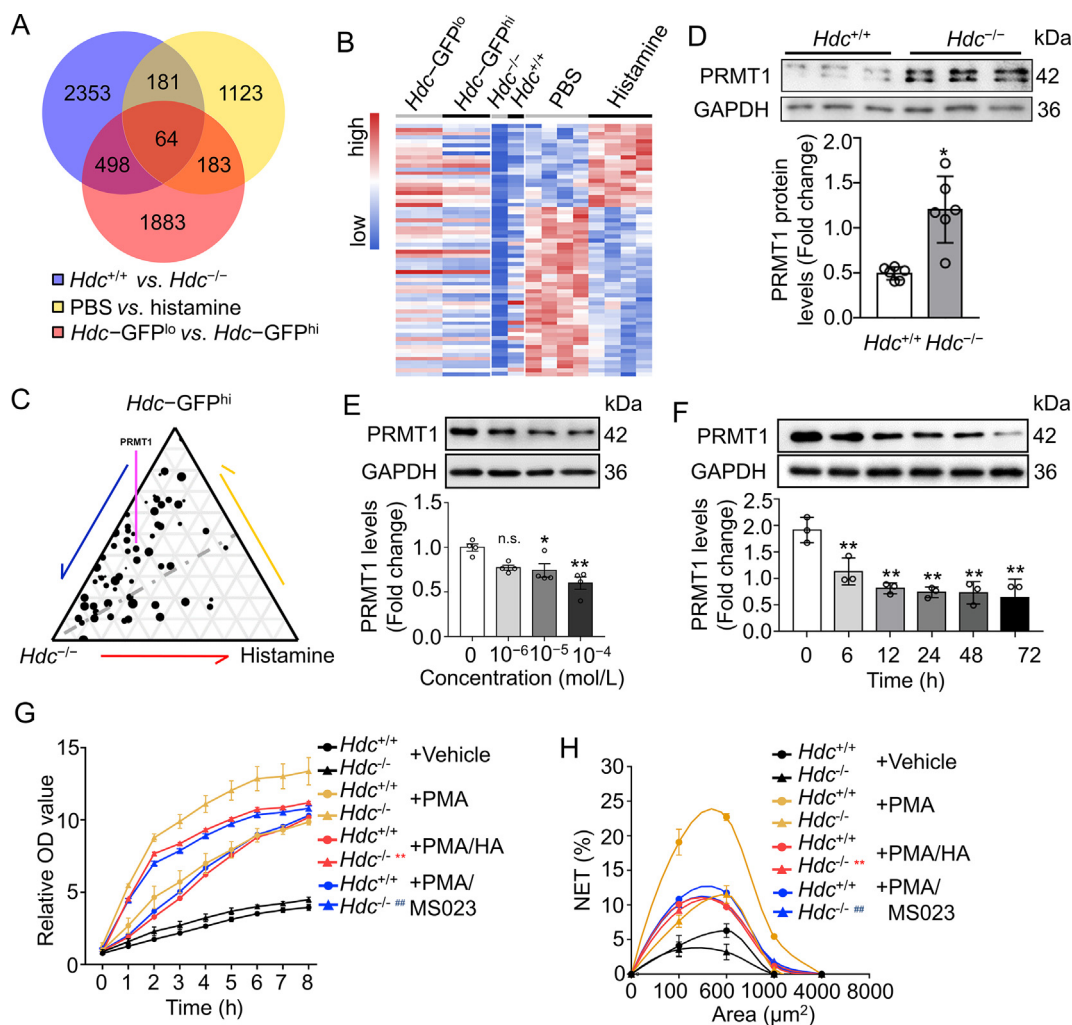


Figure 5 PRMT1 is negatively regulated by histamine in myeloid cells. (A) The Venn diagram shows the numbers of significantly DEGs in the paired groups of *Hdc*^{-/-} vs. *Hdc*^{+/+} myeloid cells (blue), with vs. without histamine treated myeloid cells (yellow), *Hdc* high expressed (*Hdc*-GFP^{hi}) vs. following *Hdc* low expressed (*Hdc*-GFP^{lo}) myeloid cells (red). 64 DEGs were identified in all three paired groups. (B) The heatmaps of the shared 64 DEGs from the above three paired groups. (C) Triangle plot shows the increased/decreased expression of the 64 DEGs in the indicated groups. (D) The representative images of Western blots of the protein levels of PRMT1 in neutrophils isolated from the bone marrow of *Hdc*^{-/-} and *Hdc*^{+/+} mice ($n = 6$). Data are shown as mean \pm SEM. * $P < 0.05$ vs. vehicle group. (E) The representative images of Western blots of the protein levels of PRMT1 in HL60 cells treated with the indicated doses of histamine for 24 h ($n = 3$). Data are shown as mean \pm SEM. * $P < 0.05$, ** $P < 0.01$ vs. vehicle group; n.s. no significant. (F) The representative images of Western blots of the protein levels of PRMT1 in HL60 cells treated with 10⁻⁴ mol/L histamine for the indicated time ($n = 3$). Data are shown as mean \pm SEM. ** $P < 0.01$ vs. vehicle group. (G) The relative ROS levels produced in neutrophils from *Hdc*^{-/-} and *Hdc*^{+/+} mice were determined after the treatment of PMA along with histamine (HA) or PRMT1 inhibitor (MS023). ** $P < 0.01$, *Hdc*^{-/-} + PMA vs. *Hdc*^{-/-} + PMA/HA; ## $P < 0.01$, *Hdc*^{-/-} + PMA vs. *Hdc*^{-/-} + PMA/MS023. Data are shown as mean \pm SEM ($n = 4$). (H) The areas of NETs formed by neutrophils isolated from *Hdc*^{-/-} and *Hdc*^{+/+} mice were calculated after the treatment of PMA along with HA or MS023. ** $P < 0.01$, *Hdc*^{-/-} + PMA vs. *Hdc*^{-/-} + PMA/HA; ## $P < 0.01$, *Hdc*^{-/-} + PMA vs. *Hdc*^{-/-} + PMA/MS023. Data are shown as mean \pm SEM ($n = 4$).

Kyoto Encyclopedia of Genes and Genomes (KEGG) analysis of the differentially expressed proteins revealed that proteins with ADMA regulated by histamine were mainly enriched in the cellular process of endocytosis, RNA processing, DNA replication, and amino acid degradation (Fig. 7C). GO analysis indicated that proteins with ADMA regulated by histamine were enriched for autophagy and Golgi vesicle transport (Fig. 7D). Moreover, these proteins were enriched in mitochondrial, nuclear, and cell cortex regions of the cell (Fig. 7E), and their functions were focused on GTP binding, phosphatidylinositol phosphate binding, and nucleoside binding (Fig. 7F).

Furthermore, we noticed that 42 members of the Ras family were enriched in the proteins pulled down by the ADMA antibody (Table 1), among which 15 members were reported to be involved in ROS production. Significantly, 7 out of the 42 members, especially Rap1, the key component of NADPH oxidase, were specifically enriched in the untreated group but disappeared in the histamine-treated group. The AMDA modification of Rap1 was significantly reduced in histamine treated group (Fig. S4B), suggesting Rap1 was likely the downstream target of HDC-PRMT1 signal in regulating the ROS generation and NETs formation.

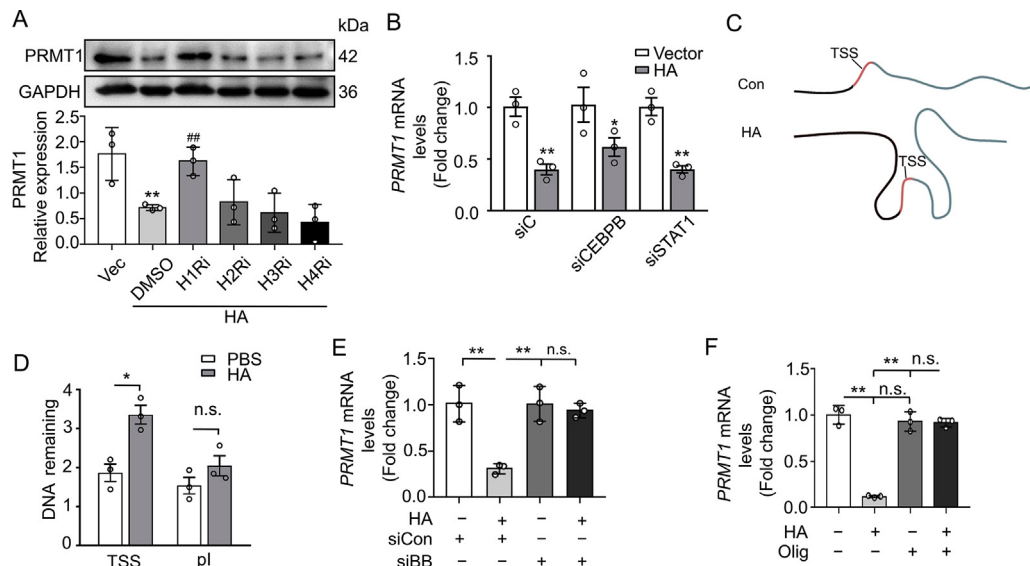


Figure 6 Histamine repressed the transcription of PRMT1 through restricting DNA accessibility of the TSS region of PRMT1. (A) HL60 cells were stimulated with histamine (100 $\mu\text{mol/L}$) for 12 h in the presence of specific antagonists for H1 receptor (pyrilamine, 10 $\mu\text{mol/L}$), H2 receptor (cimetidine, 10 $\mu\text{mol/L}$), H3 receptor (thioperamide, 10 $\mu\text{mol/L}$), or H4 receptor (JNJ-7777120, 10 $\mu\text{mol/L}$). HA, histamine. Data are shown as mean \pm SEM ($n = 4$). ** $P < 0.01$ vs. vector group; ## $P < 0.01$ vs. HA treated group. (B) HL60 cells were transfected with siRNA of scramble control (siC or siCon), *CEBPB* (siCEBPB), or *STAT1* (siSTAT1), along with HA treatment. The mRNA levels of *PRMT1* were analyzed by qRT-PCR ($n = 3$). Data are shown as mean \pm SEM. * $P < 0.05$, ** $P < 0.01$ vs. vector group. (C) Schematic of the *PRMT1* locus containing transcription start site (TSS, red) and the later part (blue). Con, control. (D) HL60 cells were treated with or without 10^{-4} mol/L HA for 12 h. DNase sensitivity assay was performed on the TSS and the intron of prior locus (pl) of *PRMT1*. The statistical results are shown as mean \pm SEM ($n = 3$). * $P < 0.05$. (E) The mRNA levels of *PRMT1* in HL60 treated with HA and/or oligomycin were determined by qRT-PCR. $n = 3$. ** $P < 0.01$. (F) HL60 cells were transfected with siC, BRG1/BRM (siBB), along with HA treatment. The mRNA levels of *PRMT1* were analyzed by qRT-PCR ($n = 3$). ** $P < 0.01$; n.s., no significant.

3.8. Inhibiting the activity of PRMT1 can rescue the aggravation of myocardial injury caused by *Hdc* deficiency after MI

The above findings implied that *Hdc* deficiency was deleterious to heart function after MI, possibly through upregulating PRMT1, leading to promoted ROS generation and excessive NETosis. Thus, to evaluate the role of PRMT1 in cardiac function after MI, *Hdc*^{-/-} mice were intravenously injected with histamine or the inhibitor of PRMT1 (MS023) before and after MI operation. Echocardiography showed that the decreased EF and FS in *Hdc*^{-/-} mice were partially rescued by treatment with MS023 and histamine on Day 7 after surgery (Fig. 8A, B and C). Meanwhile, Masson trichrome staining revealed that pretreatment with histamine and MS023 significantly slowed the process of fibrosis in *Hdc*^{-/-} mice after MI (Fig. 8D and Supporting Information Fig. S5A).

Next, the levels of ADMA and the MPO/DNA complex, which is a measure of NETosis, were detected by ELISA in the plasma of *Hdc*^{-/-} mice with or without surgery. The levels of ADMA and NETs were greatly augmented in *Hdc*^{-/-} mice after MI and could be reduced by pretreatment with histamine and MS023 to a level similar to that in *Hdc*^{+/+} mice after MI (Fig. 8E, Fig. S5B and C). Moreover, the levels of NETs were positively related to the levels of ADMA (Fig. 8F), suggesting that the pathway of asymmetric arginine dimethylation of proteins, which was the main function of PRMT1, indeed contributed to the increased NETs observed in *Hdc*^{-/-} mice.

4. Discussion

Despite the development of percutaneous coronary intervention (PCI), the prognosis of patients with ST-segment elevation myocardial infarction (STEMI) varies greatly⁵⁰. The different immune responses of patients to the ischemic injury during the early phase contribute to the diversity of clinical pathological progress⁵¹. However, little is known about the intrinsic regulators of immune cells that influence inflammatory responses to myocardial injury. This study revealed that *Hdc*/histamine regulated neutrophil mobilization and limited additional reactive oxidative species and NET generation after myocardial infarction by the H1R–SWI/SNF–PRMT1 pathway (Fig. 9). Our findings identify a new mechanism for neutrophil dependent inflammation and provide a rationale for neutrophils as a therapeutic target for acute myocardial infarction.

The expression of *Hdc* in the bone marrow has been shown to decrease across the lifespan, implicating its immunological role in aging related diseases⁵² (Supporting Information Fig. S6). Previous data have shown that *Hdc*/histamine participates in regulating the progression of acute heart injury⁵³ and heart failure¹⁷, but the underlying mechanisms have not been fully unveiled. Here, we illustrated the transcriptional profile of the injured hearts of *Hdc*^{-/-} mice on Days 0, 1, and 7 after ligation of the left anterior descending coronary artery. Time course analysis of GO showed that immunological phenomena was closely related to the progression of MI and that the immune state in the heart changed along with the development of myocardial remodeling. Immune recruitment analysis indicated that immunocytes, neutrophils especially,

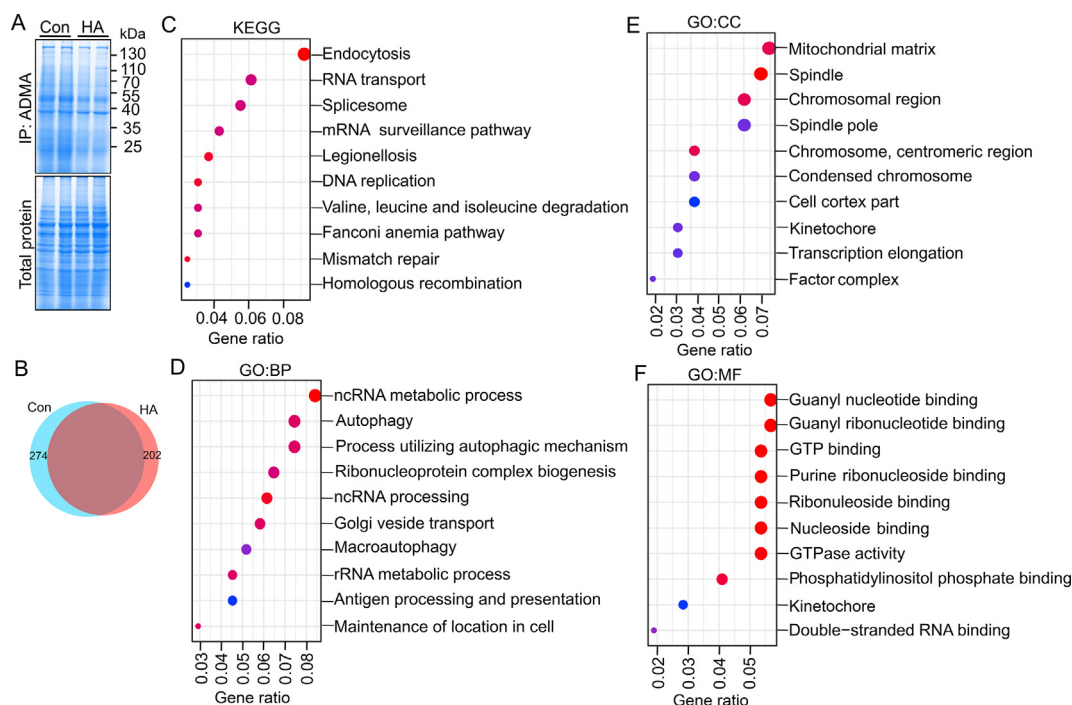


Figure 7 The asymmetric dimethylated arginine (ADMA) profiling of PRMT1 targets were regulated by HA. (A) Coomassie blue staining of proteins with ADMA from HL60 cells with/without HA treatment. (B) The Venn diagram shows the proteins with ADMA in control and HA treated groups. 274 proteins were detected uniquely in the control group and 202 proteins uniquely in the HA treated group. (C) KEGG pathway enrichment analysis for the differentially expressed proteins uniquely detected in control and HA treated groups. The Rich ratio of x -axis refers to the ratio of selected gene numbers annotated in this pathway terms to all gene numbers annotated in this pathway term. The calculating formula is Rich ratio = term candidate gene number/term gene number. The size and color of the bubbles represent the number of differentially expressed proteins enriched in the pathway and enrichment significance, respectively. (D–F) GO of BP (D), CC (E), and MF (F). Enrichment analysis of histamine regulated proteins with ADMA modification were shown. The size and color of the bubbles represent the number of differentially expressed proteins enriched in the pathway and enrichment significance, respectively.

infiltrated infarcted hearts within a different time frame in *Hdc*^{-/-} mice, compared with *Hdc*^{+/+} mice. *Hdc* deficiency greatly increased the counts of neutrophils in the myocardium on Days 3 and 7 after MI.

Although *Hdc* was globally knockout in our experiments, our previous data had suggested that the expression of HDC in myocardium is extremely low to be detected (data not shown) and there were no abnormalities in the cardiac structure and function of *Hdc*^{-/-} mice under normal conditions. Moreover, neutralizing Ly6G⁺ neutrophils ameliorated the prognosis of MI in *Hdc*^{-/-} mice in the present work, which suggested the contributing role of neutrophils in the aggravated cardiac function loss in *Hdc*^{-/-} mice with MI.

Neutrophils are vital for clearing pathogens or debris in acute inflammation. However, in the context of MI, abnormal neutrophils are detrimental to cardiac function. Clinically, the neutrophil-to-lymphocyte ratio has been employed to predict the survival of patients with STEMI and the improvement of coronary artery disease events is found to be correlated with neutrophil reduction⁵⁴. These findings suggest that neutrophils to be a potential target for the treatment of myocardial infarction. Here, we first reveal that *Hdc*/histamine is an endogenous factor involved in regulating the infiltration of neutrophils into the heart after MI.

Our data showed that the migration of neutrophils was reinforced in *Hdc*^{-/-} mice after MI, in accordance with the

phenomenon of infectious inflammation described previously. Surprisingly, the adhesion of *Hdc*^{-/-} neutrophils to endothelial cells was decreased. Histamine has been reported to activate endothelial cells by promoting the expression of adhesion related genes, but the role of histamine in the adhesion of neutrophils is still unknown. In *Hdc*^{-/-} mice, with the increased migration but the decreased neutrophil adhesion, why the infiltrated neutrophils were significantly increased on Days 3 and 7, but not on Day 1 after injury is the next scientific question we are eager to answer. Moreover, it will be interesting to analyze the effect of *Hdc* on neutrophils at the earlier stage such as 1, 3, 6, or 12 h post MI, as the adhesion of neutrophils affected the recruitment at the start of inflammation.

Oxidative burst is the way of neutrophils that eliminate pathogens or respond to inflammatory stimuli. Histamine is thought to inhibit ROS driven by opsonized zymosan particles or fMLP in a PKC-independent way^{55,56}. Our data showed that deletion of *Hdc* led to neutrophils in a hyperoxidative state not only under the treatment of PMA, an agonist of PKC, but also in the baseline state.

NETosis is a unique mechanism of cell death in neutrophils driven by ROS with various stimulations. It has been reported that NETs lead to the death of cells by histones^{9,57,58}. In addition, NETs have recently been reported to promote fibrosis²⁷ and cell activation/proliferation⁵⁹ by neutrophil elastase (NE) dependent

Table 1 ADMA proteins of the RAS family related to ROS.

Group	ADMA protein ^a	ROS
Only in Con	RAP1B ³⁶	↑
	RIN3, RAB15, RAB18, RAB5B, RAB6A, RAP2A	—
Both in Con and HA	RAP1A ³⁷	↑
	G3BP1 ³⁸	↑
	IQGAP1 ³⁹	↑
	RAC1 ³⁹	↑
	RAC2 ⁴⁰	↑
	RAB10 ⁴¹	↑
	RAB27A ⁴²	↑
	RAB35 ⁴³	↑
	ARF6 ⁴⁴	↑
	CDC42 ⁴⁵	↓
	RASA3 ⁴⁶	↓
	RAB31 ⁴⁷	↓
	ARF4 ⁴⁸	↓
	RASSF2, IQGAP2, RAB11A, RAB14, RAB1A, RAB1B, RAB21, RAB2A, RAB32, RAB5A, RAB5C, RAB6B, RAB7A, RAB8A, ARF5, ARF3, RALA	—
	Only in HA	NRAS ⁴⁹
AK3, RAB8B, RAB8B		—

^aThe ADMA proteins of RAS family are divided into 3 groups: only in control (Con), both in Con and histamine (HA) groups, and only in HA group. Their roles in ROS production are indicated as arrows. ↑ represents the gene promotes the production of ROS; ↓ presents the gene decreases the production of ROS.

matrix remodeling. Herein, *in vivo* experiments revealed that excessive NETs accompanied with augmented cardiac injury after MI in *Hdc*^{-/-} mice. Our data showed that cardiomyocyte death and fibroblast proliferation/migration were aggravated by *Hdc*^{-/-} NETs. These findings indicate that aggregated neutrophils, which migrate into the heart, may promote cell death of the myocardium, expand the injured zone, and pave the way for fibroblasts rather than purging cell debris or reducing inflammation⁶⁰.

To clarify the underlying mechanisms through which *Hdc*/histamine regulated ROS generation and the formation of NETs, we analyzed the DEGs regulated by *Hdc*, by combining our transcriptomic data and the published transcriptomic data of myeloid cells in the GEO database. After screening, we found that the expression of PRMT1 was tightly repressed by HDC/histamine at the mRNA and protein levels, while rescued by the antagonist of H1R. PRMT1 is an important enzyme responsible for asymmetric arginine dimethylation. It has been reported that there is a negative correlation between histamine and methylation in the serum of patients with behavioral disorders⁶¹. In the current study, histamine treatment, which repressed the transcriptional level of *PRMT1*, reduced the level of proteins with ADMA modification, which is consistent with the phenomenon observed in behavioral disorders patients⁶¹. Moreover, inhibiting the catalytic activity of PRMT1 by MS023 could limit the excessive ROS generation and NETosis, and improve the cardiac function of *Hdc*^{-/-} mice post MI, suggesting that the effect of PRMT1 on NETosis and MI mediated by HDC/histamine-PRMT1 signaling is dependent on its catalytic activity of arginine methylation.

STAT1 and CEBPB have been reported to be responsible for the regulation of *PRMT1* transcription in fibroblasts^{33,34,62}. However, in our work, the data showed that neither transcription factor participated in the regulation of histamine on *PRMT1* expression. This may be due to the different kinds of cell types. Instead, histamine repressed *PRMT1* transcription by restricting DNA accessibility to its TSS region through ATP-dependent chromatin remodeling. Chromatin remodeling occurs in the process of cell differentiation⁶³, while PRMT1 has been reported to participate in the maintenance of short-term hematopoietic stem cells, which implies that PRMT1 may participate in histamine-induced myeloid cell maturation. This suggested that ATP analogues or inhibitors of enzymes of chromatin remodeling are the potential targets to modulate PRMT1 expression and NETosis. Beside that histamine repressed the transcription of *PRMT1* through restricting the DNA accessibility to the TSS region of *PRMT1*, our results of co-IP revealed that PRMT1 and HDC could interact with each other slightly, which was not affected by histamine or MS023 treatment as shown in Fig. S6B and C. The phenomenon aroused an interesting question that besides for the catalytic activity of arginine methylation, would PRMT1 act on HDC in a novel way as a negative feedback regulation of histamine inhibiting PRMT1 transcription? Or may PRMT1 and HDC form a complex with other proteins to function in cells? These questions need more efforts to figure out in the future work.

Type I PRMTs, including PRMT1–4, PRMT6, and PRMT8, promote ADMA, reducing the positive charge and hydrophilicity of proteins³¹. Many published studies certified that this type of modification involved in multiple cell activities, including gene transcription, cell signaling, mRNA translation, DNA damage signaling, protein trafficking, protein stability, and pre-mRNA splicing^{32,64–66}. Previous study implicated that the deficiency of *Ddah1*, which is the key enzyme for ADMA degradation, raised ROS levels in cardiomyocytes. Moreover, it has also been reported that ADMA promotes ROS generation in macrophages⁶⁷ and MPO release in polymorphonuclear neutrophils in the context of cardiovascular disease⁶⁸. In our work, the levels of ADMA were shown to be positively related to the levels of NETs in a mouse model of MI, implying that the ADMA playing a role in regulating ROS generation and the formation of NETs.

Although Pyun et al.⁶⁹ reported that mice null for cardiac PRMT1 could exhibit dilated cardiomyopathy after 2 months, there is no other work exploring the role of PRMT1 during acute MI up to now. Our work revealed that the expression of PRMT1 in neutrophils would be increased but showed no significant change in myocardium after *Hdc* deletion. Inhibiting PRMT1 could limit the excessive ROS generation and NETosis in *Hdc*-deficient neutrophils, improving the cardiac function of *Hdc*^{-/-} mice post MI. Similarly, directly reducing neutrophils could also attenuate cardiac injury post MI in *Hdc*^{-/-} mice. Based on these, we consider that PRMT1 mainly in neutrophils played a potential role in regulating the aggravated cardiac injury post MI in *Hdc*^{-/-} mice. Our results and the work of Pyun et al.⁶⁹ suggested that PRMT1 likely possess different functions in different cells and different diseases models.

To determine the downstream factor of PRMT1 in regulating the formation of NETs, the ADMA modified profiling of proteins were determined by mass spectrometry in our work. GTP binding and GTPase activity were specifically enriched in the histamine

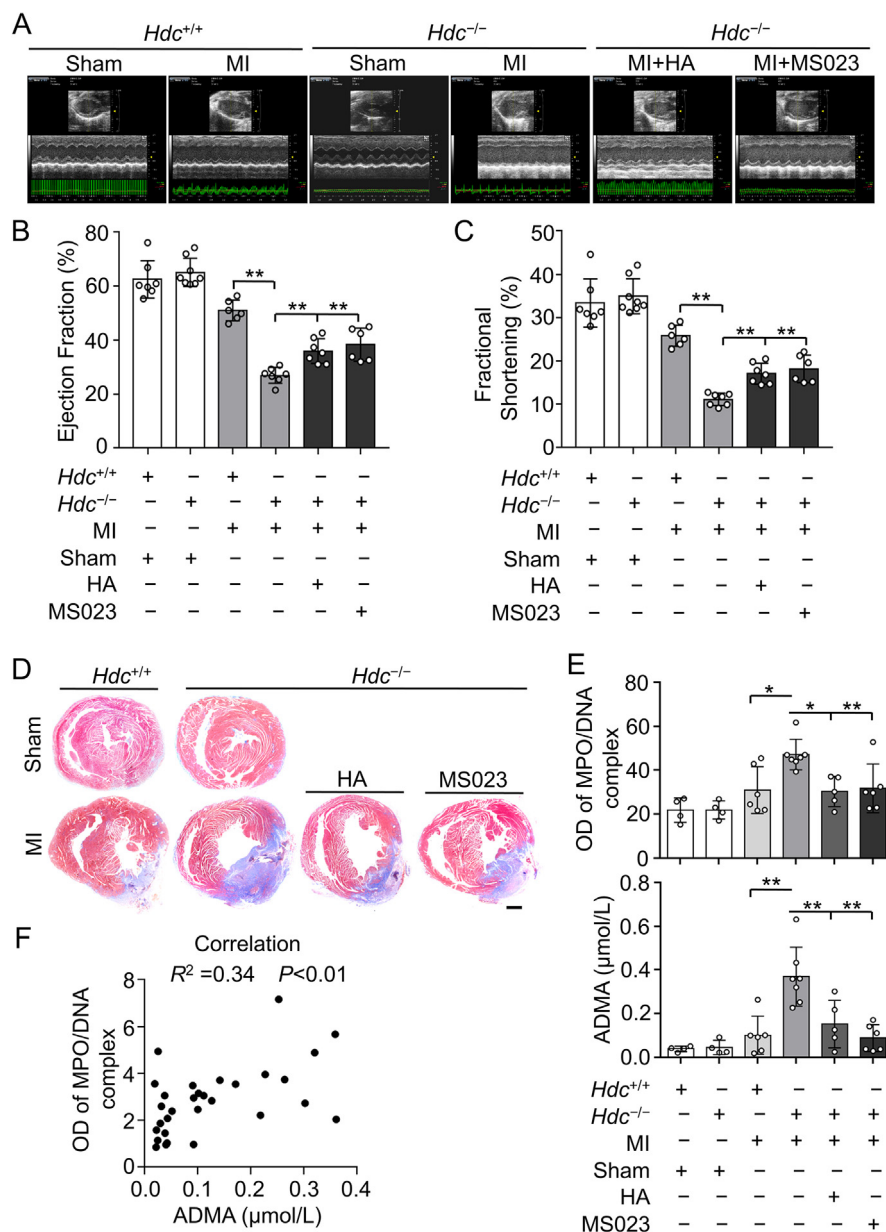


Figure 8 Inhibiting the activity of PRMT1 can rescue the aggravation of myocardial injury caused by *Hdc* deficiency after MI. (A) Representative echocardiographic images of *Hdc*^{-/-} and *Hdc*^{+/+} mice on Day 7 after ligation. *Hdc*^{-/-} and *Hdc*^{+/+} mice were intravenous injected with HA or MS023 prior to surgery. (B and C) Quantitation of LVEF and FS of *Hdc*^{-/-} and *Hdc*^{+/+} mice 7 days after infarction. $n = 6-8$ mice in each group. Data are shown as mean \pm SEM. $**P < 0.01$. (D) Representative images of Masson staining of hearts from *Hdc*^{-/-} and *Hdc*^{+/+} mice. *Hdc*^{-/-} and *Hdc*^{+/+} mice were intravenous injected with HA or MS023 prior to surgery. Scale bar, 50 μ m. (E) MPO/DNA and ADMA levels in plasma from *Hdc*^{-/-} and *Hdc*^{+/+} mice on Day 7 after ligation were determined by ELISA according to the manual instructions. *Hdc*^{-/-} and *Hdc*^{+/+} mice were intravenous injected with HA or MS023 prior to surgery. Data are shown as mean \pm SEM. $*P < 0.05$, $**P < 0.01$, $n = 6-8$ mice in each group. (F) Correlation of MPO/DNA and ADMA levels in plasma from *Hdc*^{-/-} and *Hdc*^{+/+} mice on Day 7 after ligation. *Hdc*^{-/-} and *Hdc*^{+/+} mice were intravenous injected with HA or MS023 prior to surgery. $R^2 = 0.34$, $P < 0.01$. Data are shown as mean \pm SEM, $n = 30$.

untreated group. In neutrophils, NADPH oxidase is the main complex responsible for ROS generation. It contains catalytic gp91phox (also known as NOX2), regulatory components, p22phox, p40phox, p47phox, p67phox, and Rac/Rap1^{70,71}. Rac/Rap1, belongs to the Ras family, many members of which are involved in the regulation of ROS (Table 1). The hydrophilicity of Rap1 would be reduced by its ADMA modification, which may

facilitate its localization to the NADPH-oxidase complex on the membrane of mitochondria. The reduction of the ADMA modification of Rap1 caused by histamine suggested the downstream role of Rap1 in HDC-PRMT1 signaling. Taken together, our findings strongly suggested that the activity of NADPH oxidase could be regulated by PRMT1 to promote ROS production and NET formation, indicating that NADPH oxidase or Rap1 could

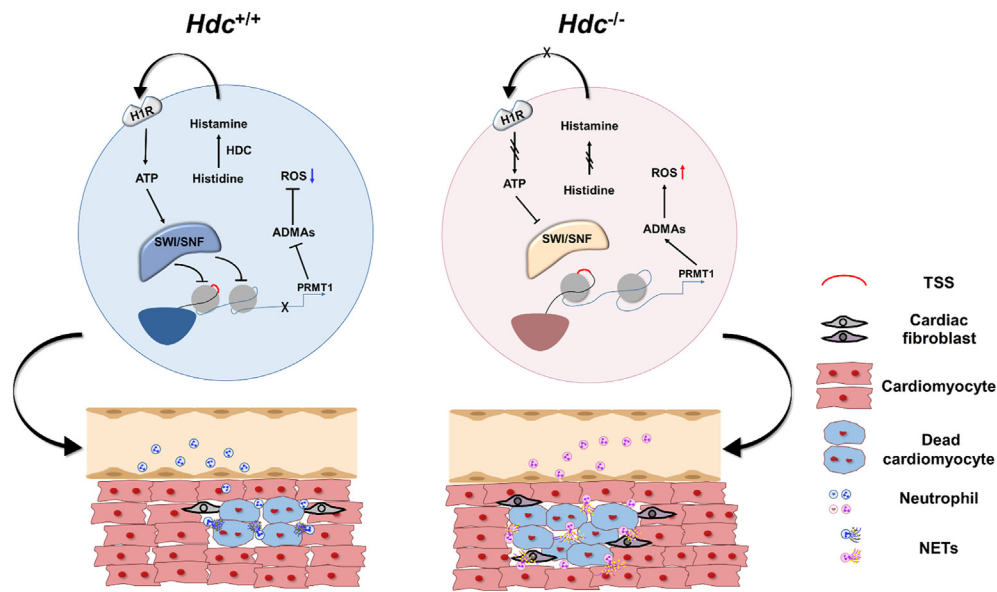


Figure 9 Schematic illustration of the effect of HDC on neutrophils after MI. In neutrophils, autocrine, paracrine, or exogenous of histamine, by activating histamine H1 receptor, repress PRMT1 expression, ADMA production, and ROS generation by ATP–SWI/SNF dependent chromatin remodeling. After MI, the deletion of *Hdc*, without endogenous or exogenous histamine, aggravates cardiomyocyte death and fibrosis, by enhanced neutrophil infiltration and ROS dependent NETosis.

also be the potential target for the immune modulation for the cardiovascular disease.

5. Conclusions

Our study demonstrates that the lack of *Hdc* promotes NETosis by the H1R–SWI/SNF–PRMT1–ROS pathway, and hence leads to aggravated cardiomyocyte death and fibroblast activation. Targeting any one of them may provide insights into new treatments for myocardial infarction and consequent cardiac remodeling. These findings improve our understanding of the significant role of neutrophil and NET formation in cardiovascular disease and provide new biomarkers and pharmaceutical targets for identifying and tuning the detrimental immune state in cardiovascular disease.

Acknowledgments

This study was supported by grants from the National Key Research and Development Plan (2016YFC1101102, China), the National Natural Science Foundation of China (81521001 and 81500262), the Basic Research Project of Shanghai Committee of Science and Technology (19JC1411400, China), and the Laboratory Animal Science Foundation of Shanghai Committee of Science and Technology (19140902000, China).

Author contributions

Zhiwei Zhang, Suling Ding, Zhe Wang, Xiangdong Yang, and Junbo Ge were involved in the study design, data analysis, and manuscript preparation. Zhiwei Zhang, Suling Ding, Zhe Wang, Zheliang Zhou, Xiaowei Zhu, Weiwei Zhang, and Zhe Wang performed the experiments. All authors reviewed the manuscript.

Conflicts of interests

The authors declare no competing conflict of interest.

Appendix A. Supporting information

Supporting data to this article can be found online at <https://doi.org/10.1016/j.apsb.2021.10.016>.

References

- Ding S, Abudupataer M, Zhou Z, Chen J, Li H, Xu L, et al. Histamine deficiency aggravates cardiac injury through miR-206/216b-Atg13 axis-mediated autophagic-dependant apoptosis. *Cell Death Dis* 2018; **9**:694.
- Opie LH, Commerford PJ, Gersh BJ, Pfeffer MA. Controversies in ventricular remodelling. *Lancet* 2006; **367**:356–67.
- Frantz S, Bauersachs J, Ertl G. Post-infarct remodelling: contribution of wound healing and inflammation. *Cardiovasc Res* 2009; **81**:474–81.
- Silvestre-Roig C, Braster Q, Ortega-Gomez A, Soehnlein O. Neutrophils as regulators of cardiovascular inflammation. *Nat Rev Cardiol* 2020; **17**:327–40.
- Leoni G, Soehnlein O. (Re) solving repair after myocardial infarction. *Front Pharmacol* 2018; **9**:1342.
- Curaj A, Schumacher D, Rusu M, Staudt M, Li X, Simsekylmaz S, et al. Neutrophils modulate fibroblast function and promote healing and scar formation after murine myocardial infarction. *Int J Mol Sci* 2020; **21**:3685.
- Brinkmann V, Reichard U, Goosmann C, Fauler B, Uhlemann Y, Weiss DS, et al. Neutrophil extracellular traps kill bacteria. *Science* 2004; **303**:1532–5.
- Warnatsch A, Ioannou M, Wang Q, Papayannopoulos V. Neutrophil extracellular traps license macrophages for cytokine production in atherosclerosis. *Science* 2015; **349**:316–20.
- Yu Y, Su K. Neutrophil extracellular traps and systemic lupus erythematosus. *J Clin Cell Immunol* 2013; **4**:139.

10. Middleton EA, He XY, Denorme F, Campbell RA, Ng D, Salvatore SP, et al. Neutrophil extracellular traps contribute to immunothrombosis in COVID-19 acute respiratory distress syndrome. *Blood* 2020;**136**:1169–79.
11. Liu J, Yang D, Wang X, Zhu Z, Wang T, Ma A, et al. Neutrophil extracellular traps and dsDNA predict outcomes among patients with ST-elevation myocardial infarction. *Sci Rep* 2019;**9**:11599.
12. Mangold A, Alias S, Scherz T, Hofbauer T, Jakowitsch J, Panzenböck A, et al. Coronary neutrophil extracellular trap burden and deoxyribonuclease activity in ST-elevation acute coronary syndrome are predictors of ST-segment resolution and infarct size. *Circ Res* 2015;**116**:1182–92.
13. Chen X, Deng H, Churchill MJ, Luchsinger LL, Du X, Chu TH, et al. Bone marrow myeloid cells regulate myeloid-biased hematopoietic stem cells via a histamine-dependent feedback loop. *Cell Stem Cell* 2017;**21**:747–60. e747.
14. Yang XD, Ai W, Asfaha S, Bhagat G, Friedman RA, Jin G, et al. Histamine deficiency promotes inflammation-associated carcinogenesis through reduced myeloid maturation and accumulation of CD11b⁺ Ly6G⁺ immature myeloid cells. *Nat Med* 2011;**17**:87–95.
15. Ding S, Abudupataer M, Zhou Z, Chen J, Li H, Xu L, et al. Histamine deficiency aggravates cardiac injury through miR-206/216b–Atg13 axis-mediated autophagic-dependant apoptosis. *Cell Death Dis* 2018;**9**:694.
16. Ohtsu H, Tanaka S, Terui T, Hori Y, Makabe-Kobayashi Y, Pejler G, et al. Mice lacking histidine decarboxylase exhibit abnormal mast cells. *FEBS Lett* 2001;**502**:53–6.
17. Chen J, Hong T, Ding S, Deng L, Abudupataer M, Zhang W, et al. Aggravated myocardial infarction-induced cardiac remodeling and heart failure in histamine-deficient mice. *Sci Rep* 2017;**7**:44007.
18. Gao E, Lei YH, Shang X, Huang ZM, Zuo L, Boucher M, et al. A novel and efficient model of coronary artery ligation and myocardial infarction in the mouse. *Circ Res* 2010;**107**:1445–53.
19. Zhou Z, Zhang S, Ding S, Abudupataer M, Zhang Z, Zhu X, et al. Excessive neutrophil extracellular trap formation aggravates acute myocardial infarction injury in apolipoprotein E deficiency mice via the ROS-dependent pathway. *Oxid Med Cell Longev* 2019;**2019**:1209307.
20. Ackers-Johnson M, Li PY, Holmes AP, O'Brien SM, Pavlovic D, Foo RS. A simplified, Langendorff-free method for concomitant isolation of viable cardiac myocytes and nonmyocytes from the adult mouse heart. *Circ Res* 2016;**119**:909–20.
21. Kessenbrock K, Fröhlich L, Sixt M, Lämmermann T, Pfister H, Bateman A, et al. Proteinase 3 and neutrophil elastase enhance inflammation in mice by inactivating antiinflammatory progranulin. *J Clin Invest* 2008;**118**:2438–47.
22. Kukulski F, Yebdri FB, Lecka J, Kauffenstein G, Lévesque SA, Martín-Satué M, et al. Extracellular ATP and P2 receptors are required for IL-8 to induce neutrophil migration. *Cytokine* 2009;**46**:166–70.
23. Rezaazadeh S, Yang D, Tomblin G, Simon M, Regan SP, Seluanov A, et al. SIRT6 promotes transcription of a subset of NRF2 targets by mono-ADP-ribosylating BAF170. *Nucleic Acids Res* 2019;**47**:7914–28.
24. Shi Y, Shi H, Nieman DC, Hu Q, Yang L, Liu T, et al. Lactic acid accumulation during exhaustive exercise impairs release of neutrophil extracellular traps in mice. *Front Physiol* 2019;**10**:709.
25. Arslan F, de Kleijn DP, Timmers L, Doevendans PA, Pasterkamp G. Bridging innate immunity and myocardial ischemia/reperfusion injury: the search for therapeutic targets. *Curr Pharmaceut Des* 2008;**14**:1205–16.
26. Hori Y, Nihei Y, Kurokawa Y, Kuramasu A, Makabe-Kobayashi Y, Terui T, et al. Accelerated clearance of *Escherichia coli* in experimental peritonitis of histamine-deficient mice. *J Immunol* 2002;**169**:1978–83.
27. Martinod K, Witsch T, Erpenbeck L, Savchenko A, Hayashi H, Cherpokova D, et al. Peptidylarginine deiminase 4 promotes age-related organ fibrosis. *J Exp Med* 2017;**214**:439–58.
28. Hofbauer TM, Mangold A, Scherz T, Seidl V, Panzenböck A, Ondracek AS, et al. Neutrophil extracellular traps and fibrocytes in ST-segment elevation myocardial infarction. *Basic Res Cardiol* 2019;**114**:33.
29. Chrysanthopoulou A, Mitroulis I, Apostolidou E, Arelaki S, Mikroulis D, Konstantinidis T, et al. Neutrophil extracellular traps promote differentiation and function of fibroblasts. *J Pathol* 2014;**233**:294–307.
30. Kiffin R, Grauers Wiktorin H, Nilsson MS, Aurelius J, Aydin E, Lenox B, et al. Anti-leukemic properties of histamine in monocytic leukemia: the role of NOX2. *Front Oncol* 2018;**8**:218.
31. Blanc RS, Richard S. Arginine methylation: the coming of age. *Mol Cell* 2017;**65**:8–24.
32. He X, Zhu Y, Lin YC, Li M, Du J, Dong H, et al. PRMT1-mediated FLT3 arginine methylation promotes maintenance of FLT3-ITD⁺ acute myeloid leukemia. *Blood* 2019;**134**:548–60.
33. Sun Q, Liu L, Mandal J, Molino A, Stolz D, Tamm M, et al. PDGF-BB induces PRMT1 expression through ERK1/2 dependent STAT1 activation and regulates remodeling in primary human lung fibroblasts. *Cell Signal* 2016;**28**:307–15.
34. Sun Q, Fang L, Tang X, Lu S, Tamm M, Stolz D, et al. TGF- β upregulated mitochondria mass through the SMAD2/3 \rightarrow C/EBP β \rightarrow PRMT1 signal pathway in primary human lung fibroblasts. *J Immunol* 2019;**202**:37–47.
35. Ji L, Zhao X, Zhang B, Kang L, Song W, Zhao B, et al. Slc6a8-mediated creatine uptake and accumulation reprogram macrophage polarization via regulating cytokine responses. *Immunity* 2019;**51**:272–84. e277.
36. Vara DS, Campanella M, Canobbio I, Dunn WB, Pizzorno G, Hirano M, et al. Autocrine amplification of integrin α Ib β 3 activation and platelet adhesive responses by deoxyribose-1-phosphate. *Thromb Haemostasis* 2013;**109**:1108–19.
37. Li Y, Kim JG, Kim HJ, Moon MY, Lee JY, Kim J, et al. Small GTPases Rap1 and RhoA regulate superoxide formation by Rac1 GTPases activation during the phagocytosis of IgG-opsonized zymosans in macrophages. *Free Radic Biol Med* 2012;**52**:1796–805.
38. Cho E, Than TT, Kim SH, Park ER, Kim MY, Lee KH, et al. G3BP1 depletion increases radiosensitization by inducing oxidative stress in response to DNA damage. *Anticancer Res* 2019;**39**:6087–95.
39. Mo CF, Li J, Yang SX, Guo HJ, Liu Y, Luo XY, et al. IQGAP1 promotes anoikis resistance and metastasis through Rac1-dependent ROS accumulation and activation of Src/FAK signalling in hepatocellular carcinoma. *Br J Cancer* 2020;**123**:1154–63.
40. Raad H, Mouawia H, Hassan H, El-Seblani M, Arabi-Derkawi R, Boussetta T, et al. The protein kinase A negatively regulates reactive oxygen species production by phosphorylating gp91phox/NOX2 in human neutrophils. *Free Radic Biol Med* 2020;**160**:19–27.
41. Wauters F, Cornelissen T, Imberechts D, Martin S, Koentjoro B, Sue C, et al. LRRK2 mutations impair depolarization-induced mitophagy through inhibition of mitochondrial accumulation of RAB10. *Autophagy* 2020;**16**:203–22.
42. Luo Y, Yu MH, Yan YR, Zhou Y, Qin SL, Huang YZ, et al. Rab27A promotes cellular apoptosis and ROS production by regulating the miRNA-124-3p/STAT3/RelA signalling pathway in ulcerative colitis. *J Cell Mol Med* 2020;**24**:11330–42.
43. Deng W, Wang Y, Gu L, Duan B, Cui J, Zhang Y, et al. MICAL1 controls cell invasive phenotype via regulating oxidative stress in breast cancer cells. *BMC Cancer* 2016;**16**:489.
44. Bourmoum M, Charles R, Claing A. The GTPase ARF6 controls ROS production to mediate angiotensin II-induced vascular smooth muscle cell proliferation. *PLoS One* 2016;**11**:e0148097.
45. Diebold BA, Fowler B, Lu J, Dinauer MC, Bokoch GM. Antagonistic cross-talk between Rac and Cdc42 GTPases regulates generation of reactive oxygen species. *J Biol Chem* 2004;**279**:28136–42.
46. Hartman ES, Brindley EC, Papoin J, Ciciotte SL, Zhao Y, Peters LL, et al. Increased reactive oxygen species and cell cycle defects contribute to anemia in the RASA3 mutant mouse model *scat*. *Front Physiol* 2018;**9**:689.

47. Zhang KQ, Chu XD. GANT61 plays antitumor effects by inducing oxidative stress through the miRNA-1286/RAB31 axis in osteosarcoma. *Cell Biol Int* 2021;**45**:61–73.
48. Eun SY, Jang HS, Kang ES, Kim GH, Kim HJ, Lee JH, et al. Identification of ADP-ribosylation factor 4 as a suppressor of *N*-(4-hydroxyphenyl) retinamide-induced cell death. *Cancer Lett* 2009;**276**:53–60.
49. Ye F, Chai W, Xie M, Yang M, Yu Y, Cao L, et al. HMGB1 regulates erastin-induced ferroptosis via RAS–JNK/p38 signaling in HL-60/NRASQ61L cells. *Am J Cancer Res* 2019;**9**:730.
50. Cavender MA, Milford-Beland S, Roe MT, Peterson ED, Weintraub WS, Rao SV. Prevalence, predictors, and in-hospital outcomes of non-infarct artery intervention during primary percutaneous coronary intervention for ST-segment elevation myocardial infarction (from the National Cardiovascular Data Registry). *Am J Cardiol* 2009;**104**:507–13.
51. Mayadas TN, Tsokos GC, Tsuboi N. Mechanisms of immune complex-mediated neutrophil recruitment and tissue injury. *Circulation* 2009;**120**:2012–24.
52. Schaum N, Lehallier B, Hahn O, Pálóvics R, Hosseinzadeh S, Lee SE, et al. Ageing hallmarks exhibit organ-specific temporal signatures. *Nature* 2020;**583**:596–602.
53. Deng L, Hong T, Lin J, Ding S, Huang Z, Chen J, et al. Histamine deficiency exacerbates myocardial injury in acute myocardial infarction through impaired macrophage infiltration and increased cardiomyocyte apoptosis. *Sci Rep* 2015;**5**:13131.
54. Ridker PM, Thuren T, Zalewski A, Libby P. Interleukin-1 β inhibition and the prevention of recurrent cardiovascular events: rationale and design of the Canakinumab Anti-inflammatory Thrombosis Outcomes Study (CANTOS). *Am Heart J* 2011;**162**:597–605.
55. Romero AI, Thorén FB, Brune M, Hellstrand K. NKp46 and NKG2D receptor expression in NK cells with CD56dim and CD56bright phenotype: regulation by histamine and reactive oxygen species. *Br J Haematol* 2006;**132**:91–8.
56. Vasicek O, Lojek A, Jancinova V, Nosal R, Ciz M. Role of histamine receptors in the effects of histamine on the production of reactive oxygen species by whole blood phagocytes. *Life Sci* 2014;**100**:67–72.
57. Zhang Y, Jian W, He L, Wu J. Externalized histone H4: a novel target that orchestrates chronic inflammation by inducing lytic cell death. *Acta Biochim Biophys Sin (Shanghai)* 2020;**52**:336–8.
58. Saffarzadeh M, Juenemann C, Queisser MA, Lochnit G, Barreto G, Galuska SP, et al. Neutrophil extracellular traps directly induce epithelial and endothelial cell death: a predominant role of histones. *PLoS One* 2012;**7**:e32366.
59. Albrengues J, Shields MA, Ng D, Park CG, Ambrico A, Poindexter ME, et al. Neutrophil extracellular traps produced during inflammation awaken dormant cancer cells in mice. *Science* 2018;**361**:eaao4227.
60. Schauer C, Janko C, Munoz LE, Zhao Y, Kienhöfer D, Frey B, et al. Aggregated neutrophil extracellular traps limit inflammation by degrading cytokines and chemokines. *Nat Med* 2014;**20**:511–7.
61. Walsh WJ, Glab LB, Haakenson ML. Reduced violent behavior following biochemical therapy. *Physiol Behav* 2004;**82**:835–9.
62. Jin A, Tang X, Zhai W, Li Y, Sun Q, Liu L, et al. TSLP-induced collagen type-I synthesis through STAT3 and PRMT1 is sensitive to calcitriol in human lung fibroblasts. *Biochim Biophys Acta Mol Cell Res* 2021;**1868**:119083.
63. Piazza F, Semenzato G. Molecular therapeutic approaches to acute myeloid leukemia: targeting aberrant chromatin dynamics and signal transduction. *Expert Rev Anticancer Ther* 2004;**4**:387–400.
64. Hartel NG, Chew B, Qin J, Xu J, Graham NA. Deep protein methylation profiling by combined chemical and immunoaffinity approaches reveals novel PRMT1 targets. *Mol Cell Proteomics* 2019;**18**:2149–64.
65. Liu LM, Sun WZ, Fan XZ, Xu YL, Cheng MB, Zhang Y. Methylation of C/EBP α by PRMT1 inhibits its tumor-suppressive function in breast cancer. *Cancer Res* 2019;**79**:2865–77.
66. Jeong MH, Jeong HJ, Ahn BY, Pyun JH, Kwon I, Cho H, et al. PRMT1 suppresses ATF4-mediated endoplasmic reticulum response in cardiomyocytes. *Cell Death Dis* 2019;**10**:903.
67. Chen CH, Zhao JF, Hsu CP, Kou YR, Lu TM, Lee TS. The detrimental effect of asymmetric dimethylarginine on cholesterol efflux of macrophage foam cells: role of the NOX/ROS signaling. *Free Radic Biol Med* 2019;**143**:354–65.
68. von Leitner EC, Klinke A, Atzler D, Slocum JL, Lund N, Kielstein JT, et al. Pathogenic cycle between the endogenous nitric oxide synthase inhibitor asymmetrical dimethylarginine and the leukocyte-derived hemoprotein myeloperoxidase. *Circulation* 2011;**124**:2735–45.
69. Pyun JH, Kim HJ, Jeong MH, Ahn BY, Vuong TA, Lee DI, et al. Cardiac specific PRMT1 ablation causes heart failure through CaMKII dysregulation. *Nat Commun* 2018;**9**:5107.
70. Panday A, Sahoo MK, Osorio D, Batra S. NADPH oxidases: an overview from structure to innate immunity-associated pathologies. *Cell Mol Immunol* 2015;**12**:5–23.
71. Ferro E, Goitre L, Retta SF, Trabalzini L. The interplay between ROS and Ras GTPases: physiological and pathological implications. *J Signal Transduct* 2012;**2012**:365769.